Transcriptomic Profiling of Control and Thyroid-Associated Orbitopathy (TAO) Orbital Fat and TAO Orbital Fibroblasts Undergoing Adipogenesis

Dong Won Kim,[1] Kamil Taneja,[2] Thanh Hoang,[1] Clayton P. Santiago,[1] Timothy J. McCulley,[2] Shannath L. Merbs,[3] Nicholas R. Mahoney,[2] Seth Blackshaw,[1,2,4–6] and Fatemeh Rajaii[2]

[1]Solomon H. Snyder Department of Neuroscience, Johns Hopkins University School of Medicine, Baltimore, Maryland, United States
[2]Department of Ophthalmology, Wilmer Eye Institute, Johns Hopkins University School of Medicine, Baltimore, Maryland, United States
[3]Department of Ophthalmology and Visual Sciences, University of Maryland School of Medicine, Baltimore, Maryland, United States
[4]Department of Neurology, Johns Hopkins University School of Medicine, Baltimore, Maryland, United States
[5]Institute for Cell Engineering, Johns Hopkins University School of Medicine, Baltimore, Maryland, United States
[6]Kavli Neuroscience Discovery Institute, Johns Hopkins University School of Medicine, Baltimore, Maryland, United States

PURPOSE. Orbital fat hyperplasia commonly occurs in thyroid-associated orbitopathy (TAO). To understand molecular mechanisms underlying orbital adipogenesis, we used transcriptomics to compare gene expression in controls and patients with TAO, as well as in orbital fibroblasts (OFs) undergoing adipogenic differentiation.

METHODS. We performed bulk RNA sequencing (RNA-Seq) on intraconal orbital fat from controls and patients with TAO. We treated cultured OFs derived from patients with TAO with adipogenic media to induce adipogenesis. We used single nucleus RNA-Seq (snRNA-Seq) to profile treated and control OFs, identifying genes that are dynamically expressed during orbital adipogenesis in vitro, and compared these results to data from control and TAO orbital fat.

RESULTS. Gene expression profiles in control and TAO orbital fat are distinct. Signaling pathways including PI3K-Akt signaling, cAMP signaling, AGE-RAGE signaling, regulation of lipolysis, and thyroid hormone signaling are enriched in orbital fat isolated from patients with TAO. SnRNA-Seq of orbital fibroblasts undergoing adipogenesis reveals differential expression of the adipocyte-specific genes *FABP4/5*, *APOE*, *PPARG*, and *ADIPOQ* during adipogenic differentiation. The insulin-like growth factor-1 receptor and Wnt signaling pathways appear to be enriched early in adipogenesis. Gene modules that are enriched in TAO orbital fat are upregulated in orbital adipocytes during differentiation in vitro, whereas genes that are enriched in control orbital fat are enriched in undifferentiated OFs.

CONCLUSIONS. We identified pathways enriched in TAO orbital fat, and dynamic changes in gene expression that occur during adipogenic differentiation of orbital fibroblasts. These findings may help guide functional studies of genes and pathways critical for orbital adipogenesis.

Keywords: thyroid associated orbitopathy, Graves' disease, orbital fat, adipogenesis, orbital fibroblasts

Thyroid-associated orbitopathy (TAO) is a form of autoimmune thyroid disease in which shared auto-antigens in the thyroid gland and orbit are targets of the immune response.[1–3] About 25% of patients with autoimmune thyroid disease will develop ocular disease, which can be vision-threatening. It is thought that inflammatory signaling causes expansion of the orbital soft tissues due to fibrosis and orbital fat hyperplasia which causes ocular morbidity due to corneal exposure and/or compressive optic neuropathy.[4–6]

The orbital soft tissue expansion that causes vision loss and other ocular morbidity associated with TAO is thought to be the final step of an inflammatory cascade that results in fibrosis and adipogenesis. Details of the mechanisms underlying orbital adipogenesis are not well understood. Generally, adipogenesis is initiated by transcription factor cascades involving transient early expression of CCAAT/enhancer-binding protein (C/EBP) -β and -δ followed by induction of CEBP-α and peroxisome proliferator-activated receptor γ, transcription factors, which in turn induce expression

TABLE. Characteristics of TAO and Control Patients Undergoing Orbital Surgery

	Control S1	Control S2	Control S3	TAO S1	TAO S2	TAO S3
Age (years)	>70	58	>70	37	51	51
Gender	M	M	F	F	F	M
Race	Asian	C	C	C	AA	AA
Duration of thyroid disease prior to surgery (approx. mo)	N/A	N/A	N/A	48	13	13
Duration of TED prior to surgery (approx. mo)	N/A	N/A	N/A	18	13	10
Previous treatment for Graves' disease	N/A	N/A	N/A	Armor thyroid	Methimazole	Carbimazole
Previous treatment for TED	N/A	N/A	N/A	N/A	N/A	Prednisone, Methylpred-nisolone, Azathioprine
Smoking history	>10 years ago	No	No	Former	No	No
Exophthalmometry, Hertel (mm)	N/A	N/A	N/A	21	27.5	30
Presence of compressive optic neuropathy	N/A	N/A	N/A	No	No	Yes
Surgery	Excision of orbital fat prolapse	Excision of orbital fat prolapse	Primary Enucleation (UM)	Orbital decom-pression	Orbital decom-pression	Orbital decom-pression
Clinical Activity Score (0-7)	N/A	N/A	N/A	0	1	3

AA, African American; C, Caucasian; N/A, not applicable; UM, uveal melanoma.

of genes involved in terminal adipocyte differentiation.[7,8] These pathways contribute to a generic adipocyte differentiation program. However, adipocyte metabolic function, morphology, preadipocyte proliferation, and capacity for adipogenesis differ among adipose tissue depots.[9] These molecular and physiological differences, which have been explored in subcutaneous, visceral, and brown adipose tissue depots, are thought to be intrinsic to adipocytes and may be related to their embryonic origins.[9] The differences in orbital adipose tissue, and the way in which they may contribute to the TAO phenotype, however, have not yet been explored.

To identify molecular mechanisms controlling adipogenesis in TAO, we have conducted bulk RNA sequencing (RNA-Seq) analysis of primary orbital fat from both controls and patients with TAO, and also used single nucleus RNA-Seq (snRNA-Seq) to profile orbital fibroblasts undergoing adipogenesis in vitro.

METHODS

Bulk RNA-Seq

Human intraconal orbital fat was obtained from patients with TAO undergoing orbital decompression or controls undergoing routine resection of prolapsed orbital fat (Table), which has been shown to be intraconal fat,[10] or primary enucleation for uveal melanoma using a protocol approved by the Johns Hopkins University Institutional Review Board and following the tenets of the Declaration of Helsinki. Patients with TAO were inactive at the time of surgery, defined by a clinical activity score (CAS) less than 4.[11] Samples were placed in RNA*later*™ (#AM7020; ThermoFisher Scientific, Waltham, MA, USA), ice, or frozen fresh on dry ice, depending on the intended subsequent use. RNA was extracted from each sample using

Trizol (#15596018; ThermoFisher) and RNeasy mini kits (#74104; Qiagen, Germany). Bioanalyzer (Agilent) analysis was used to perform quality control. The cDNA libraries were prepared for samples with RIN >6. RNA-Seq libraries were made using TruSeq Stranded Total RNA kit (Illumina, San Diego, CA, USA) and libraries were sequenced using Illumina NextSeq 500 (Illumina), paired-end read of 75 bp, 50 million reads per library. Illumina adapters of libraries after sequencing were removed using Cutadapt (version 1.18)[12] with default parameters. Sequenced libraries were then aligned to GRCh38 using STAR (version 2.42a)[13] with –twopassMode Basic. RSEM (version 1.3.1)[14] was used for transcript quantification, with rsem-calculate-expression (*–forwad-prob 0.5*).

DESeq2 (version 1.24.0)[15] was used to analyze the bulk RNA-Seq dataset using the standard pipeline, filtering low counts (<10) and choosing genes with adjusted *P* value < 0.05. ClusterProfiler (version 3.12.0)[16] *enrichKEGG* function was used to identify pathways that are enriched in the TAO group.

In Vitro Differentiation

Orbital fibroblast cell lines were derived from TAO intraconal fat as previously described.[17] Briefly, tissue explants were obtained from patients undergoing surgical decompression for TAO. Patients were inactive, with a CAS less than 4, at the time of surgery.[11] Explants were placed on the bottom of culture plates and covered with Eagle's medium containing 10% FBS, antibiotics, and glutamine. They were incubated at 37°C, 5% CO_2, in a humidified environment. Media was changed weekly until the cells reached confluence. The resulting fibroblast monolayers were passaged serially by gentle treatment with TrypLE (#12604039; ThermoFisher

Scientific). Strains were stored in liquid N_2 until needed and were used between the fourth and eighth passages.

Orbital fibroblasts were induced to undergo adipogenesis as previously described.[17] Briefly, fibroblasts between passages four and eight were seeded on plastic tissue culture plates and allowed to proliferate to near-confluence in DMEM containing 10% FBS and antibiotics. The cells were then treated with adipogenic medium consisting of DMEM:F-10 (1:1, #11320033; ThermoFisher Scientific) supplemented with 3% FBS, 100 nmol/liter insulin (#12585014; ThermoFisher Scientific), 1 µmol/liter dexamethasone (#D4902; Sigma, St. Louis, MO, USA), and for the first week only, 1 µmol/liter rosiglitazone (#R2408; Sigma) and 0.2 mmol/liter IBMX (#13630S;, Cell Signalling Technology, Danvers, MA, USA). Media was changed every other day for the first week, and then twice weekly for the remaining weeks. Cultures were maintained in this medium for 21 days. Control cultures were treated with DMEM:F-10 (1:1), supplemented with 3% FBS and vehicle. Differentiation was observed using a Nikon microscope (Japan). Each time point was analyzed in triplicate.

Quantification of Adipocytes

On days 0, 5, 9, and 21, cells were washed with PBS and fixed using 4% paraformaldehyde in PBS for 10 minutes at room temperature. Cells were washed with PBS or stored in PBS at 4°C. To stain adipocytes, cells were washed with 60% isopropanol and stained with freshly prepared 0.3% (w/v) Oil red O (Sigma) at room temperature for 15 minutes. Cells were rinsed with 60% isopropanol, stained lightly with hematoxylin (Sigma) for 5 minutes, and then rinsed with PBS. Cells were imaged by a masked study team member using a Keyence BZ-X710 microscope (Keyence, Japan). Four high-power field images were obtained per replicate. Cell counts and lipid vacuole measurements were performed using ImageJ.[18] Oil red O-positive cells were counted as adipocytes and nuclei in cells that did not stain with Oil red O, which represent fibroblasts or preadipocytes, were not included in the adipocyte cell count. To quantify lipid vacuole area, images were converted to eight8-bit, and made binary using an automated algorithm, scaled to pixels and analyzed using the Analyze Particles in ImageJ.[18]

Single-Nucleus RNA-Seq

Nuclei from the treated groups were isolated at days 0, 5, 9, and 21 using the methods described in the 10x Genomics Sample Preparation Demonstrated Protocol (10x Genomics, Pleasanton, CA, USA). Nuclei from control groups were isolated at day 0, 5, and 31 using the same methods. Briefly, cells were washed with chilled PBS and lysed in chilled lysis buffer consisting of 10 mM Tris-HCl, 10 mM NaCl, 3 mM MgCl2, and 0.1% Nonidet P40 Substitute (MP Biomedicals, Solon, OH, USA) in nuclease-free water at 4°C. Cells were scraped from the plate bottom and centrifuged at 500 RCF for 5 minutes at 4°C. Cells were washed twice in nuclei wash and resuspension buffer consisting of PBS with 0.1% BSA and 0.2 U/ul RNase inhibitor (#N2615; Promega, Madison, WI, USA). Cells were passed through a 50 um CellTrics filter (#NC9491906; Sysmex, Germany) and centrifuged at 500 RCF for 5 minutes at 4°C prior to resuspension in wash and resuspension buffer. Isolated nuclei were counted manually via hemocytometer with Trypan Blue staining, and nucleus concentration was adjusted following the 10x

Genomics guideline. The 10x Genomics Chromium Single Cell system (10x Genomics) using V2 chemistry (days 0, 5, 9, and 31) or V3 chemistry (day 21) per the manufacturer's instructions, generating a total of 10 libraries. Day 5 and day 21 were run with technical replicates. Libraries were sequenced on Illumina NextSeq 500 mid-output or NovaSeq 6000 (150 million reads). Sequencing data were first preprocessed through the Cell Ranger pipeline (10x Genomics, Cellranger version 5.0.0) with default parameters, using GRCh38-2020-A genome with include-introns.

Matrix files generated from the Cellranger run were used for subsequent analysis. Seurat version 3[19] was used to perform downstream analysis, only including cells with more than 500 genes, 1000 UMI, to process control and treated samples separately. Seurat SCTransform function was used to normalize the dataset[20] and UMAP was used to reduce dimensions derived from the Harmony[21] output.

In order to identify cells that show adipocyte signatures, key adipocyte-enriched genes were first extracted from GTEx dataset from ascot.cs.jhu.edu,[22] relying on both robustness (NAUC > 20) and specificity (expressed only in both adipocytes dataset or in tissues that are enriched with adipocytes, such as mammary tissues). These genes were then used to train the dataset using Garnett[23] to identify differentiated adipocytes.

RNA velocity[24] was used to verify in vitro adipocyte differentiation trajectories. Kallisto and Bustools[25] were used to obtain splicing values, and Scanpy[26] and scVelo[27] were used to obtain velocity trajectory. Pseudotime analysis was performed using Monocle version 3[28] and genes that are significant (q value < 0.001) along pseudotime trajectory were used to run Kyoto Encyclopedia of Genes and Genomes (KEGG) analysis, as described above. Genes that were involved across KEGG signaling pathways were then used to identify signaling pathways that are specific to different stages of in vitro differentiation. SCENIC[29] was used to calculate regulons controlling gene expressions across adipocytes differentiation stages, as previously described.[30,31] Enriched genes from control and TAO bulk RNA-Seq datasets were superimposed on in vitro datasets using the Seurat *AddModuleScore* function.

Data Availability

All sequencing data are available on GEO as GSE158464 (bulk RNA-Seq dataset) and GSE174139 (bulk RNA-Seq dataset and snRNA-Seq).

RESULTS

Bulk Transcriptome Analysis of Intraconal Fat from TAO and Control Patients

Intraconal fat was collected from patients undergoing orbital surgery for TAO or other indications (Table). To compare gene expression in orbital fat in patients with TAO and controls, bulk RNA-Seq was performed (Fig. 1a). Principal component analysis (PCA) revealed that patterns of gene expression in TAO and control orbital fat segregated, with control and TAO replicates clustering together (Fig. 1b). We observed 902 genes that are enriched in control orbital fat, and 964 genes enriched in TAO orbital fat (Fig. 1c). The KEGG pathway analysis of genes enriched in TAO orbital fat revealed numerous signaling pathways that are highly enriched, including PI3K-Akt signaling, cAMP signaling,
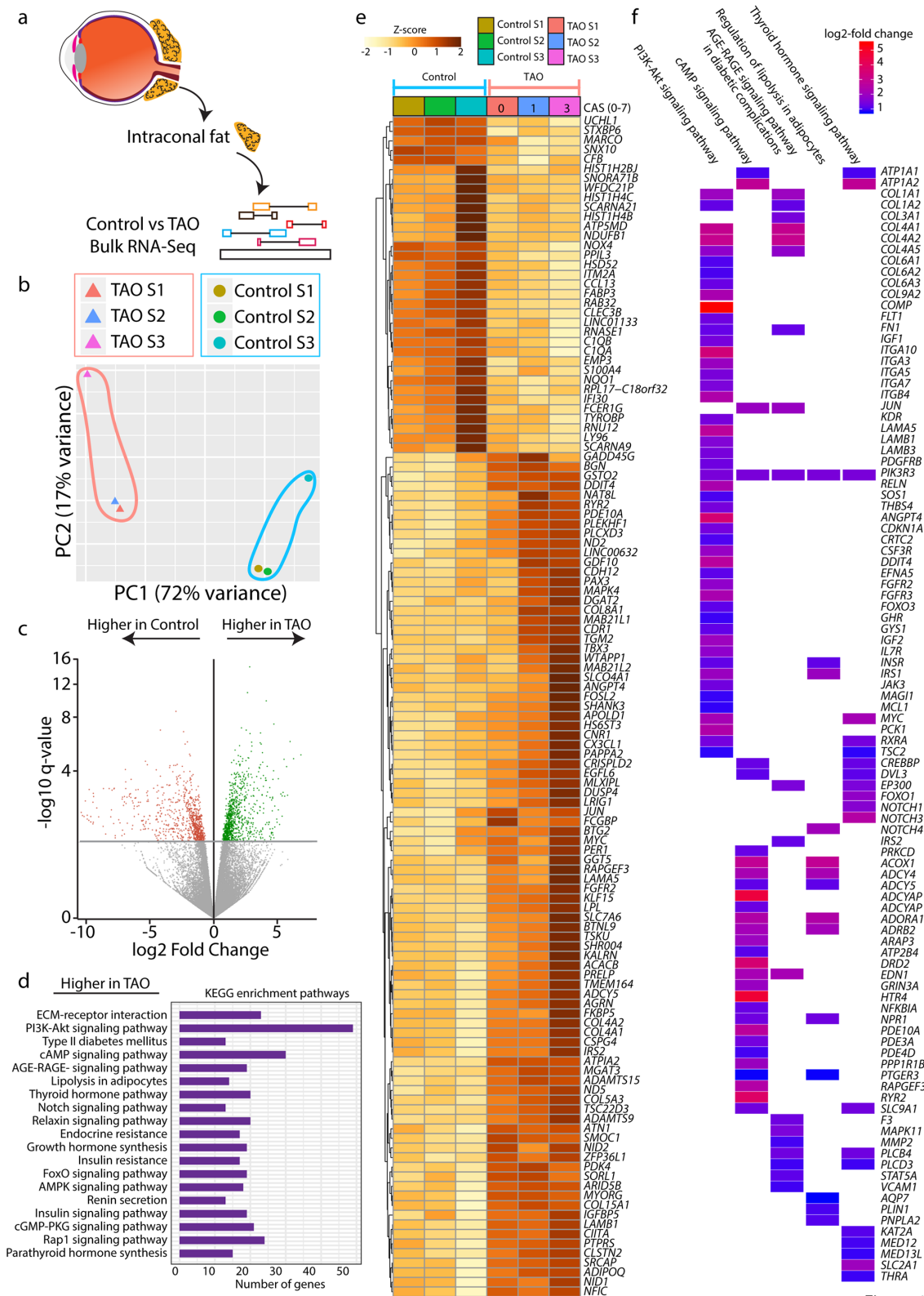
FIGURE 1. **Bulk RNA-Seq analysis comparing intraconal fat of control and TAO patients.** (**a**) Schematic diagram showing the overall experiment pipeline. (**b**) PCA plot showing the distribution of control and TAO replicates along PC1, where the axis represents a total of 72% variance, and PC2, where the axis represents a total of 17% variance. (**c**) Volcano plot of genes that are higher in control or TAO orbital fat. (**d**) KEGG pathway analysis showing pathways that are enriched in the TAO group. (**e**) Heatmap demonstrating gene expression differences between the control and TAO. (**f**) Top KEGG pathways in 1d and genes that are expressed at a higher level in TAO than in the control group log2 (Fold change). CAS = Clinical activity score.
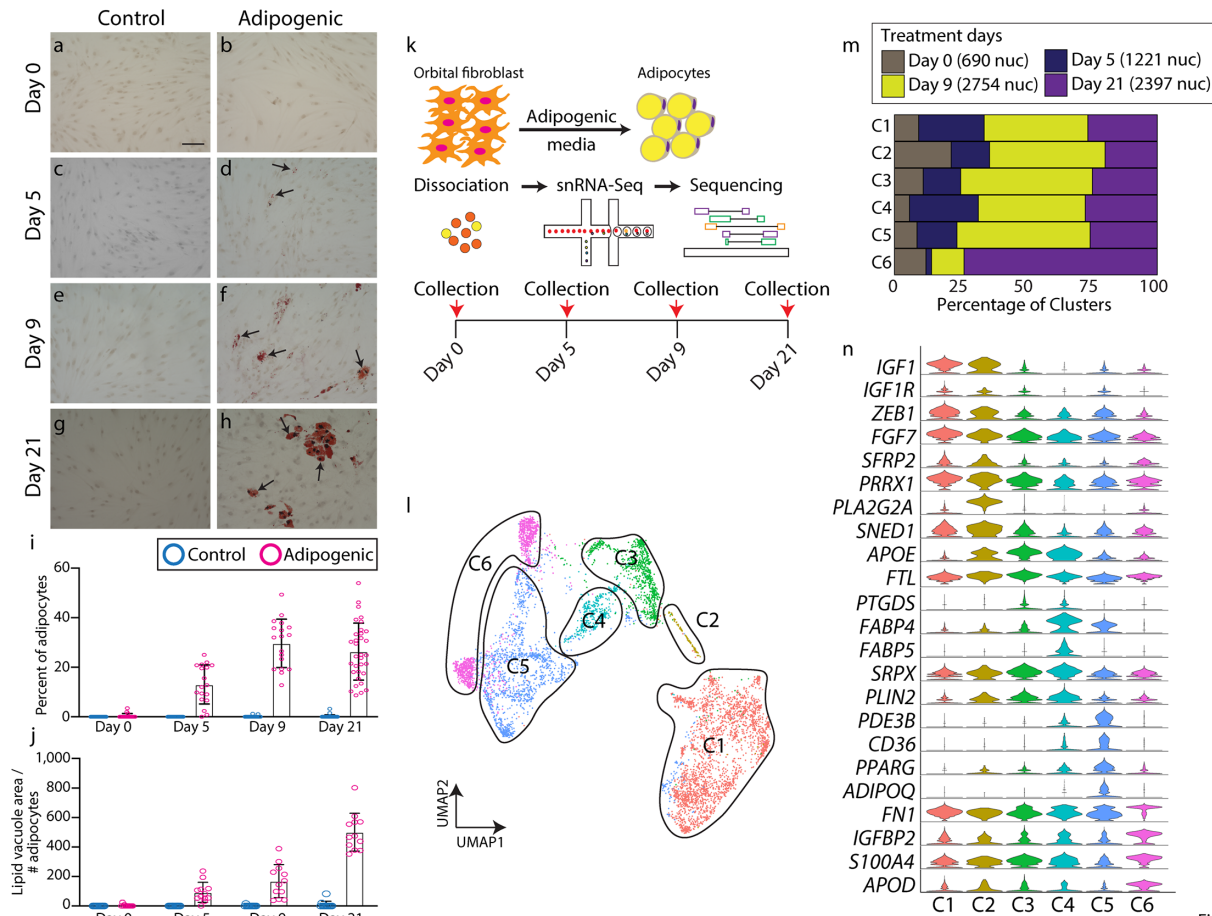
FIGURE 2.   snRNA-Seq shows adipogenesis trajectory in vitro. (a–h) Oil Red O staining (*arrows*) of orbital fibroblasts treated with control **(a, c, e, g)** and adipogenic **(b, d, f, h)** medium orbital at day 0 **(a, b)**, day 5 **(c, d)**; day 9 **(e, f)**, and day 21 **(g, h)**. **(i)** Bar plot showing the percentage of adipocytes seen after treatment with control or adipogenic medium on days 0, 5, 9, and 21. **(j)** Bar plot showing lipid vacuole area / the number of adipocytes between orbital fibroblasts treated with control or adipogenic medium on days 0, 5, 9, and 21. **(k)** Schematic diagram showing snRNA-Seq pipeline. **(l)** UMAP plot showing key six clusters of cells undergoing adipogenesis from snRNA-Seq. **(m)** Bar plot showing the percentage of clusters that are occupied across treatment days. **(n)** Violin plot showing key cluster markers. Scale bar = 100 μM.

AGE-RAGE signaling, regulation of lipolysis in adipocytes, and thyroid hormone signaling pathway (Fig. 1d). Heat map analysis of genes expressed demonstrated significant differences (adjusted *P* value < 0.05; Table S1) between TAO and control orbital fat. Correlation analysis also demonstrated that differences in gene expression levels correlate with the patient's CAS at the time of surgery (Supplementary Fig. S1, see the Table). Heat map analysis of individual genes within the above-mentioned pathways demonstrated the degree to which genes, such as *THRA* and *IGF1*, are enriched in TAO orbital fat (Fig. 1f).

snRNA-Seq of Orbital Fibroblasts Undergoing Adipogenesis Reveals Induction of Adipocyte-Specific Markers

In order to identify genes that are involved in adipogenesis in orbital fibroblasts, which may mediate the orbital fat hyperplasia seen in TAO, we used snRNA-Seq to profile differentiating orbital fibroblasts in vitro. Orbital fibroblasts

derived from case #2 were treated to induce adipogenesis over a 21-day time course. Cells treated with control media did not undergo adipogenesis (Figs. 2a,c,e,g). Based on histologic changes in cells treated with adipogenic media, we chose to analyze adipogenesis and gene expression at days 0, 5, 9, and 21 (Figs. 2a–h). Adipocyte induction first occurred between days 0 and 5, with the maximum density of adipocytes, noted at day 9 (Fig. 2i). Adipocyte maturation, as quantified by the lipid vacuole area, increased most between days 9 and 21 (Fig. 2j). We performed snRNA-Seq on orbital fibroblasts treated with control media, and did not observe any adipogenic-like cells at 0, 5 and 31 days of culture (Supplementary Fig. S2a–c, Supplementary Table S2). Furthermore, day 0 snRNA-Seq only detected fibroblast-like cells, indicating the purity of our culture condition (Supplementary Fig. S2d, Supplementary Table S3).

Based on the observed histologic changes, we collected nuclei at days 0, 5, 9, and 21 treatments for analysis by snRNA-Seq (Fig. 2k). We identified unique clusters that were enriched from day 5 onward and expressed unique sets of markers that were absent from the other clusters, such
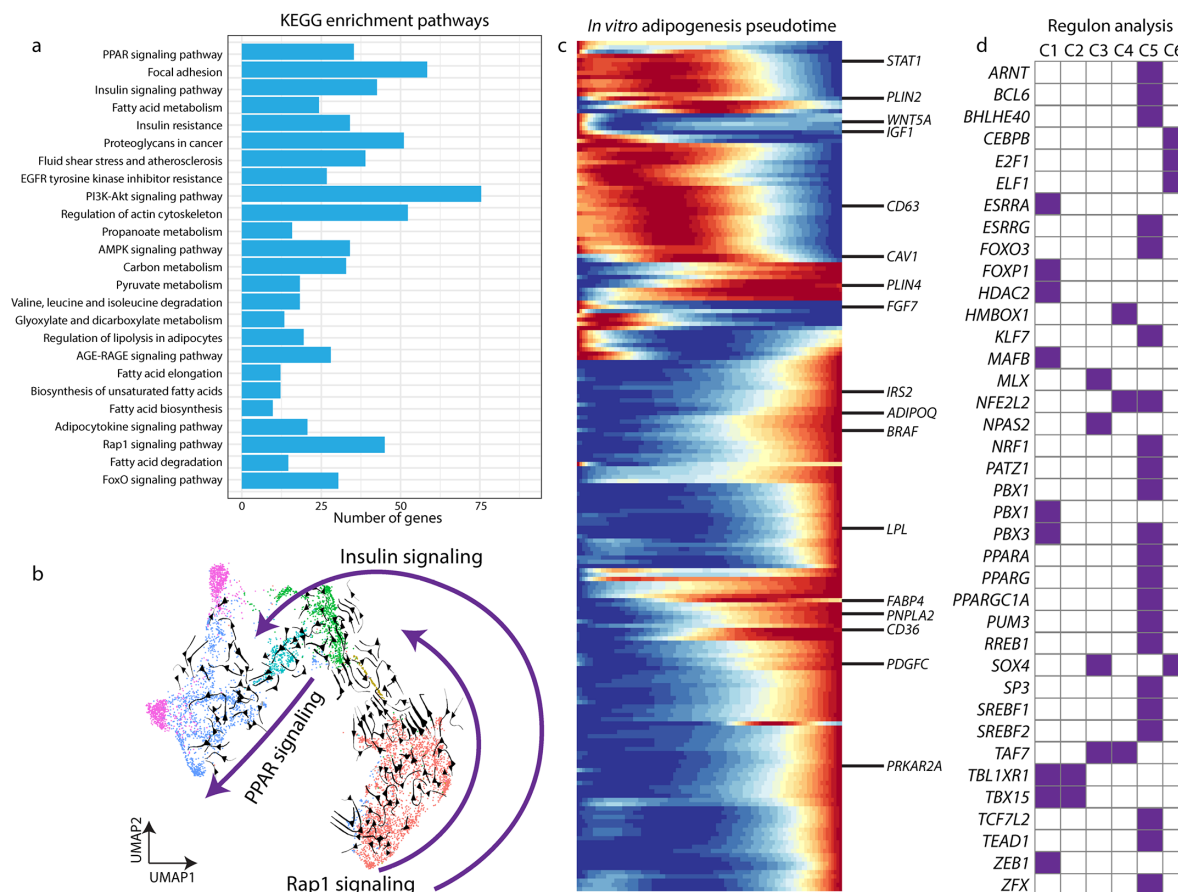
FIGURE 3. **snRNA-Seq reveals adipogenesis signaling pathway**. (**a**) KEGG plot based on pseudotime analysis from snRNA-Seq data in Figure 2. (**b**) UMAP plot with RNA velocity showing adipocyte differentiation trajectory, and three pathways that are specific across differentiation stages. (**c**) Pseudotime trajectory of adipogenesis and key genes. (**d**) Regulon analysis demonstrates key transcription factors that might be involved in each step of adipogenesis differentiation.

as *IGF1* (Supplementary Fig. S2, Supplementary Table S4). These appear to give rise to a cluster that expressed high levels of adipocyte signatures, including *ADIPOQ* (Supplementary Fig. S3, Supplementary Table S2). We identified these clusters as fibroblasts undergoing adipogenesis.

UMAP analysis of differentiating orbital fibroblasts revealed 6 distinct clusters defined by a unique set of genes (Fig. 2l). Overall, differentiating cells appeared to progress from cluster 1 (C1) to C6 over time (Fig. 2m). Classic adipocyte stem cell markers, such as *FABP4*, *APOE*, and *FABP5*, were enriched in C3 to C4, whereas mature adipocyte markers, such as *PPARG* and *ADIPOQ*, were enriched in C5, demonstrating that the clusters corresponded to a developmental progression from orbital fibroblast, through adipocyte stem cells, to mature adipocytes (Fig. 2n, Supplementary Table S5). At day 21, a new cell type was present that demonstrated high expression of *APOD*, but had lost expression of other adipogenic markers, such as *FABP4/5* but shared expression of many of the other markers expressed in other clusters were represented in cluster C6 (Fig. 2n). To identify genes that were induced early in the process of adipogenesis, we focused on genes that were specifically expressed in C1 and C2, which differed from both quiescent, control-treated orbital fibroblasts, and adipocyte stem cells. This population showed enrichment of *IGF1*, *IGF1R*, *ZEB1*, *FGF7*, and *SFRP2* expression (Fig. 2n).

Enrichment of *IGF1* expression within differentiating orbital fibroblasts suggests that paracrine signaling may be involved in the process of adipogenesis.

Analysis of Key Pathways Involved in Orbital Adipogenesis in Vitro

We next focused on identifying key signaling pathways and potential regulatory factors that are differentially expressed during orbital adipogenesis in vitro. Using KEGG analysis of the snRNA-Seq data, we observed that differentiating adipocytes express genes involved in multiple signaling pathways, including the PI3-AKT, AGE-RAGE, and insulin resistance. These pathways were also enriched in TAO orbital fat compared to control orbital fat, as measured by bulk RNA-Seq analysis (Figs. 1c, 3a). Other pathways that are specifically involved in adipogenesis, such as PPAR signaling, fatty acid biosynthesis, and fatty acid elongation (Fig. 3a) were also enriched in differentiating orbital fibroblasts.

RNA velocity analysis demonstrated that components of the Rap1 signaling pathway are active early in orbital fibroblasts in C1 (Fig. 3b). Components of the insulin signaling pathway were expressed throughout the course of adipocyte differentiation in C1 to C5 (Fig. 3b), whereas peroxisome proliferator-activated receptor (PPAR) signaling, which is
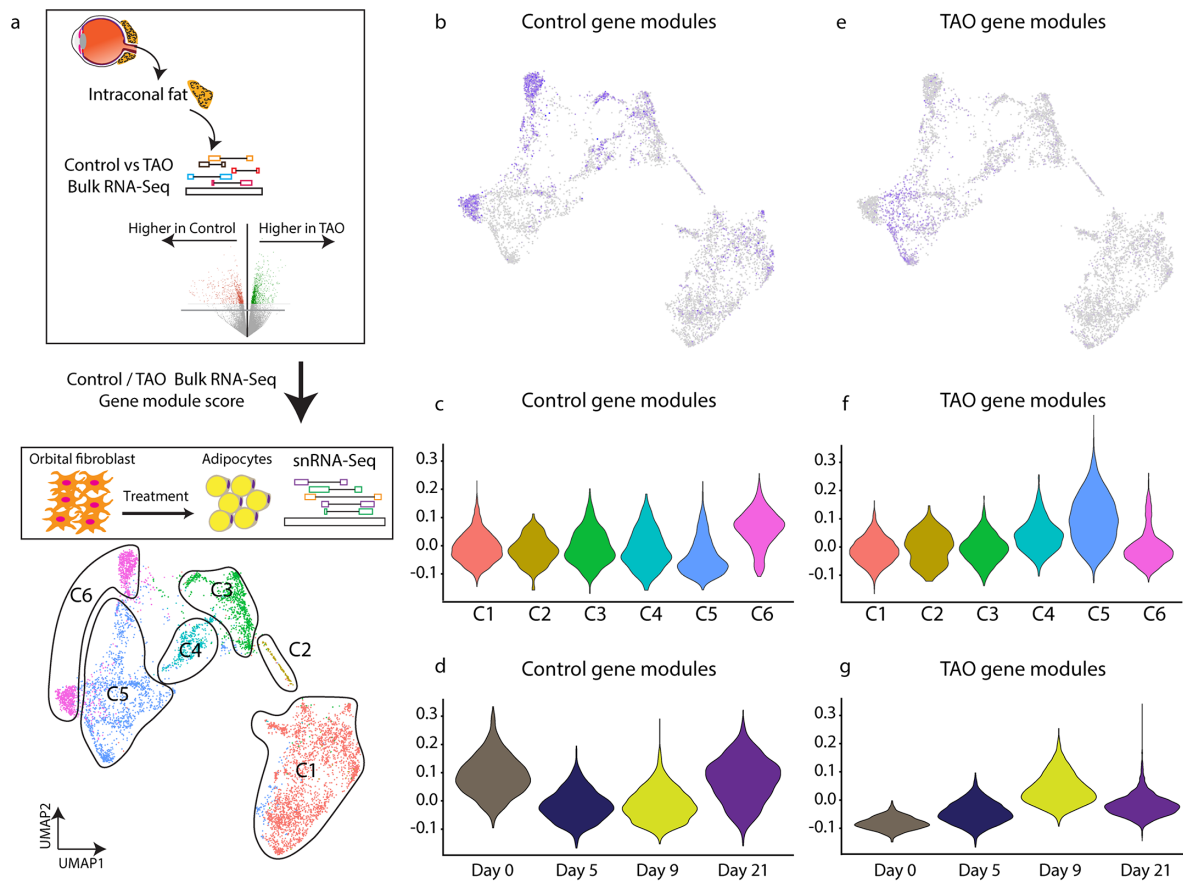
FIGURE 4. In vitro differentiated adipocytes express high levels of TAO tissue-enriched markers. (a) Schematic showing that genes that are higher in control or TAO orbital fat were projected into snRNA-Seq dataset to obtain gene module score. **(b–d)** Control intraconal fat-enriched genes demarcate cluster six in snRNA-Seq dataset **(b, d)**, expressed higher at day 0 **(c)**. **(e–g)** TAO intraconal fat-enriched genes demarcate cluster five adipocytes in snRNA-Seq dataset **(e, f)**, expressed higher at day 0 **(g)**.

known to be active late in adipogenesis, was active in C4 to C5 (Fig. 3b). Pseudotime analysis showed the progression of gene expression through C1 to C5 for all differentially expressed genes (Fig. 3c). Genes with particularly strong differential expression are highlighted, such as *IGF1*, *SFRP2*, and *WNT5A* (Fig. 3c, Supplementary Table S6). Regulon analysis identified transcription factors that are differentially expressed in each cluster (Fig. 3d).

The TAO Orbital Fat Transcriptome Resembles that of in Vitro Differentiated Adipocytes

In order to determine the similarity between in vitro derived orbital adipocytes and orbital fat in vivo, we compared gene expression from control and TAO orbital fat, analyzed by bulk RNA-Seq, to gene expression during orbital adipogenesis as assessed by snRNA-Seq (Fig. 4a). Control gene modules were found to be expressed most highly in C1 and C6. These modules were most strongly expressed in day 0 cells (C1) and a subset of day 21 cells that do not express mature adipocyte markers (C6; Figs. 4b–d). TAO gene modules were expressed most highly in C5, and at days 9 and 21 (Figs. 4e,f). Interestingly, although the orbital fibroblast cell line was derived from a patient with TAO, the gene expression pattern resembled control gene modules prior to treatment

with adipogenic media (Figs. 4c,d), and changes to resemble TAO genes modules following treatment with adipogenic media (Figs. 4f,g).

DISCUSSION

In this study, we demonstrate that orbital fibroblasts derived from patients with TAO can be used as a model to study adipogenesis in vitro. Histologic studies and transcriptome profiling clearly show that, although they are derived from patients with TAO, the gene expression profile of undifferentiated orbital fibroblasts closely resembles that of control orbital fat cells, while those treated to undergo adipogenesis display a gene expression profile more similar to that of TAO orbital fat.

We have identified signaling pathways and transcription factors that are upregulated early in orbital adipogenesis, including the insulin-like growth factor-1 (IGF-1) signaling pathway, which has previously shown to contribute to TAO pathophysiology by increasing auto-antigen display, cytokine synthesis, and hyaluronan production by orbital fibroblasts.[32,33] The novel TAO therapy teprotumumab targets the IGF-1 receptor (IGF1-R) to improve proptosis, diplopia, CAS, and quality of life in patients with TAO.[34,35] Although it is thought to exert its exerts via modulation of the immune response, our data raise the possibility that

inhibition of the IGF-1R pathway may also impact TAO by reducing adipogenesis in the orbit.

As with all transcriptomic analyses, there are limitations to this study. In particular, with the use of human tissue, there is heterogeneity in the patients' genetic background and other characteristics, which likely affect disease such as age, gender, smoking status, and CAS. Furthermore, these studies have identified very large numbers of differentially expressed genes between both control and TAO samples, and that are dynamically expressed over the course of orbital adipogenesis. Although we have focused our discussion to pathways and genes of interest based on our knowledge of TAO, there may be other pathways and genes with significant function in orbital adipogenesis and TAO.

Prior transcriptome profiling of cultured orbital fibroblasts derived from controls and patients with TAO has demonstrated significantly increased expression of homeobox transcription factors and decreased expression of Wnt signaling pathways components in TAO orbital fibroblasts.[36] In profiling TAO orbital fibroblasts undergoing adipogenesis, we find that *WNT5A* expression is high early in the course of adipogenesis, but decreases as differentiation occur, whereas homeobox gene expression increases later (Figs. 3c,d). Genes and pathways that demonstrate strong differential expression, particularly early in the process of adipogenesis, likely serve critical functions in adipogenesis, and merit further study.

The model that we have used to study gene expression changes during orbital adipogenesis depends on the treatment of orbital fibroblasts with drugs including insulin and rosiglitazone. For example, whereas cells are treated with insulin throughout the experiment, and the insulin pathway is active throughout the differentiation process, cells are also treated with the ppar-gamma agonist rosiglitazone early (during the first week) in the experiment, but PPAR signaling is active only later in the differentiation process (Fig. 3b). Thus, the dynamic gene expression that we describe is likely reflective of functional changes occurring in intracellular signaling during adipogenesis and not simply artifacts of treatment with the adipogenic media.

Microarray comparisons of orbital fat from TAO and control patients have demonstrated increased expression in Wnt signaling pathway genes, such as SFRPs, IGF-1 pathway genes, and adipogenic genes, consistent with our bulk RNA-Seq results.[37,38] In our heat map analysis of TAO-enriched genes, we note differences in the level of gene expression that correlate with CAS. Case 1, with a CAS of 0, has lower levels of TAO-enriched genes than case 2, from a patient with a CAS of 1, which in turn has lower levels of TAO-enriched genes than case 3, with CAS of 3 (Fig. 1e). However, even in the least severely affected patient, TAO-enriched genes are more highly expressed than in controls (Fig. 1e).

Other studies have compared RNA-Seq data of orbital fat from patients with active TAO compared to blepharoplasty fat and observed stronger upregulation of inflammatory signaling pathways, which is consistent with the higher CAS in their patients compared to those profiled in our study.[39] Conversely, in our patients, pathways including insulin and thyroid signaling, as well as adipogenic pathways, were more prominent, likely reflective of the patients being in earlier stages of the disease. In addition, we used intraconal fat as our control orbital adipose sample, rather than blepharoplasty fat, which may account for some of the other observed differences in gene expression. A potential confounding factor in comparing these data sets may be

that, in our analysis, we have excluded all genes with low counts due to low expression levels. Nonetheless, we also found large changes in Wnt signaling such as (*DKK2* and *NKD1*) and other pathways (*HOX3D*) in TAO orbital fat compared to control orbital fat in post hoc analysis (see Table S1), although these genes were expressed at low levels. One limitation of the transcriptomic approach is that we cannot determine the functional significance of these low levels of gene expression.

We further have identified factors that have not been previously implicated in the biology of orbital fibroblasts, including cell-autonomous pathways, such as Rap1 signaling, which have been shown to drive adipogenesis in human bone mesenchymal stem cells.[40,41] In addition, transcription factors that drive adipogenesis are of particular interest in understanding the regulation of orbital adipogenesis. ZEB1 has been identified as a critical mediator of adipogenesis in mouse pre-adipocytes and is induced by IGF-1R activation in prostate cancer cell lines.[42,43] Finally, the use of in vitro analysis of differentiating cultured orbital fibroblasts to identify pathways that regulate orbital adipogenesis, and that are enriched in TAO orbital fat, opens the possibility of using high-throughput screening to identify drug and gene-based approaches to modulating pathological adipogenesis that may ultimately be useful in treating TAO-related disorders.

Disclosure: **D.W. Kim,** None; **K. Taneja,** None; **T. Hoang,** None; **C.P. Santiago,** None; **T.J. McCulley,** None; **S.L. Merbs,** None; **N.R. Mahoney,** None; **S. Blackshaw,** CDI Labs (I, P, R), Genentech (F), Third Rock Ventures (C); **F. Rajaii,** Horizon Therapeutics (C, I)

References

1. Bahn RS, Dutton CM, Natt N, Joba W, Spitzweg C, Heufelder AE. Thyrotropin receptor expression in Graves' orbital adipose/connective tissues: potential autoantigen in Graves' ophthalmopathy. *J Clin Endocrinol Metab*. 1998;83(3):998–1002.

2. Crisp M, Lane C, Halliwell M, Wynford-Thomas D, Ludgate M. Thyrotropin Receptor Transcripts in Human Adipose Tissue [Internet]. *The Journal of Clinical Endocrinology & Metabolism*. 1997:82:2003–2005. Available from: http://dx.doi.org/10.1210/jcem.82.6.2003.

3. Porcellini A, Ruggiano G, Pannain S, et al. Mutations of thyrotropin receptor isolated from thyroid autonomous functioning adenomas confer TSH-independent growth to thyroid cells. *Oncogene*. 1997;15(7):781–789.

4. Kumar S, Coenen MJ, Scherer PE, Bahn RS. Evidence for enhanced adipogenesis in the orbits of patients with Graves' ophthalmopathy. *J Clin Endocrinol Metab*. 2004;89(2):930–935.

5. Kumar S, Iyer S, Bauer H, Coenen M, Bahn RS. A stimulatory thyrotropin receptor antibody enhances hyaluronic acid

synthesis in Graves' orbital fibroblasts: inhibition by an IGF-I receptor blocking antibody [Internet]. *J Clin Endocrinol Metab*. 2012;97:1681–1687. Available from: http://dx.doi.org/10.1210/jc.2011-2890.

6. Zhang L, Grennan-Jones F, Lane C, Rees DA, Dayan CM, Ludgate M. Adipose tissue depot-specific differences in the regulation of hyaluronan production of relevance to Graves' orbitopathy. *J Clin Endocrinol Metab*. 2012;97(2):653–662.

7. Rosen ED, Walkey CJ, Puigserver P, Spiegelman BM. Transcriptional regulation of adipogenesis. *Genes Dev*. 2000;14(11):1293–1307.

8. Rosen ED, MacDougald OA. Adipocyte differentiation from the inside out. *Nat Rev Mol Cell Biol*. 2006;7(12):885–896.

9. Hilton C, Karpe F, Pinnick KE. Role of developmental transcription factors in white, brown and beige adipose tissues. *Biochim Biophys Acta*. 2015;1851(5):686–696.

10. Tejo CR, da Costa PA, Batista RM, Rocha YRR, Borba MA. Subconjunctival fat prolapse: a disease little known to radiologists. *Radiol Bras*. 2017;50(4):272–273.

11. Mourits MP, Prummel MF, Wiersinga WM, Koornneef L. Clinical activity score as a guide in the management of patients with Graves' ophthalmopathy. *Clin Endocrinol* . 1997;47(1):9–14.

12. Martin M. Cutadapt removes adapter sequences from high-throughput sequencing reads. *EMBnet.journal*. 2011;17(1):10–12.

13. Dobin A, Davis CA, Schlesinger F, et al. STAR: ultrafast universal RNA-seq aligner. *Bioinformatics*. 2013;29(1):15–21.

14. Li B, Dewey CN. RSEM: accurate transcript quantification from RNA-Seq data with or without a reference genome. *BMC Bioinformatics*. 2011;12:323.

15. Love MI, Huber W, Anders S. Moderated estimation of fold change and dispersion for RNA-seq data with DESeq2. *Genome Biol*. 2014;15(12):550.

16. Yu G, Wang L-G, Han Y, He Q-Y. clusterProfiler: an R Package for comparing biological themes among gene clusters [Internet]. *OMICS: A Journal of Integrative Biology*. 2012;16:284–287. Available from: http://dx.doi.org/10.1089/omi.2011.0118.

17. Smith TJ, Koumas L, Gagnon A, et al. Orbital fibroblast heterogeneity may determine the clinical presentation of thyroid-associated ophthalmopathy. *J Clin Endocrinol Metab*. 2002;87(1):385–392.

18. Schneider CA, Rasband WS, Eliceiri KW. NIH Image to ImageJ: 25 years of image analysis. *Nat Methods*. 2012;9(7):671–675.

19. Stuart T, Butler A, Hoffman P, et al. Comprehensive Integration of Single-Cell Data. *Cell*. 2019;177(7):1888–1902.e21.

20. Hafemeister C, Satija R. Normalization and variance stabilization of single-cell RNA-seq data using regularized negative binomial regression. *Genome Biol*. 2019;20(1):296.

21. Korsunsky I, Millard N, Fan J, et al. Fast, sensitive and accurate integration of single-cell data with Harmony. *Nat Methods*. 2019;16(12):1289–1296.

22. Ling JP, Wilks C, Charles R, et al. ASCOT identifies key regulators of neuronal subtype-specific splicing. *Nat Commun*. 2020;11(1):137.

23. Pliner HA, Shendure J, Trapnell C. Supervised classification enables rapid annotation of cell atlases. *Nat Methods*. 2019;16(10):983–986.

24. La Manno G, Soldatov R, Zeisel A, et al. RNA velocity of single cells. *Nature*. 2018;560(7719):494–498.

25. Melsted P, Booeshaghi AS, Liu L, et al. Modular, efficient and constant-memory single-cell RNA-seq preprocessing. *Nat Biotechnol [Internet]*. 2021; Available from: http://dx.doi.org/10.1038/s41587-021-00870-2.

26. Wolf FA, Angerer P, Theis FJ. SCANPY: large-scale single-cell gene expression data analysis. *Genome Biol*. 2018;19(1):15.

27. Bergen V, Lange M, Peidli S, Wolf FA, Theis FJ. Generalizing RNA velocity to transient cell states through dynamical modeling. *Nat Biotechnol*. 2020;38(12):1408–1414.

28. Trapnell C, Cacchiarelli D, Grimsby J, et al. The dynamics and regulators of cell fate decisions are revealed by pseudotemporal ordering of single cells. *Nat Biotechnol*. 2014;32(4):381–386.

29. Aibar S, González-Blas CB, Moerman T, et al. SCENIC: single-cell regulatory network inference and clustering. *Nat Methods*. 2017;14(11):1083–1086.

30. Kim DW, Washington PW, Wang ZQ, et al. The cellular and molecular landscape of hypothalamic patterning and differentiation from embryonic to late postnatal development. *Nat Commun*. 2020;11(1):4360.

31. Kim DW, Liu K, Wang ZQ, et al. Gene regulatory networks controlling differentiation, survival, and diversification of hypothalamic Lhx6-expressing GABAergic neurons. *Commun Biol*. 2021;4(1):95.

32. Chen H, Mester T, Raychaudhuri N, et al. Teprotumumab, an IGF-1R blocking monoclonal antibody inhibits TSH and IGF-1 action in fibrocytes. *J Clin Endocrinol Metab*. 2014;99(9):E1635–E1640.

33. Chen H, Shan SJC, Mester T, Wei Y-H, Douglas RS. TSH-mediated TNFα production in human fibrocytes is inhibited by teprotumumab, an IGF-1R antagonist. *PLoS One*. 2015;10(6):e0130322.

34. Smith TJ, Kahaly GJ, Ezra DG, et al. Teprotumumab for thyroid-associated ophthalmopathy. *N Engl J Med*. 2017;376(18):1748–1761.

35. Douglas RS, Kahaly GJ, Patel A, et al. Teprotumumab for the treatment of active thyroid eye disease. *N Engl J Med*. 2020;382(4):341–352.

36. Tao W, Ayala-Haedo JA, Field MG, Pelaez D, Wester ST. RNA-sequencing gene expression profiling of orbital adipose-derived stem cell population implicate HOX genes and WNT signaling dysregulation in the pathogenesis of thyroid-associated orbitopathy. *Invest Ophthalmol Vis Sci*. 2017;58(14):6146–6158.

37. Kumar S, Leontovich A, Coenen MJ, Bahn RS. Gene expression profiling of orbital adipose tissue from patients with Graves' ophthalmopathy: a potential role for secreted frizzled-related protein-1 in orbital adipogenesis. *J Clin Endocrinol Metab*. 2005;90(8):4730–4735.

38. Ezra DG, Krell J, Rose GE, Bailly M, Stebbing J, Castellano L. Transcriptome-level microarray expression profiling implicates IGF-1 and Wnt signalling dysregulation in the pathogenesis of thyroid-associated orbitopathy. *J Clin Pathol*. 2012;65(7):608–613.

39. Lee BW, Kumar VB, Biswas P, et al. Transcriptome analysis of orbital adipose tissue in active thyroid eye disease using next generation RNA sequencing technology. *Open Ophthalmol J*. 2018;12:41–52.

40. Wu J, Cai P, Lu Z, et al. Identification of potential specific biomarkers and key signaling pathways between osteogenic and adipogenic differentiation of hBMSCs for osteoporosis therapy. *J Orthop Surg Res*. 2020;15(1):437.

41. Yeung F, Ramírez CM, Mateos-Gomez PA, et al. Nontelomeric role for Rap1 in regulating metabolism and protecting against obesity. *Cell Rep*. 2013;3(6):1847–1856.

42. Gubelmann C, Schwalie PC, Raghav SK, et al. Identification of the transcription factor ZEB1 as a central component of the adipogenic gene regulatory network. *Elife*. 2014;3:e03346.

43. Graham TR, Zhau HE, Odero-Marah VA, et al. Insulin-like growth factor-I–dependent up-regulation of ZEB1 drives epithelial-to-mesenchymal transition in human prostate cancer cells [Internet]. *Cancer Research*. 2008;68:2479–2488. Available from: http://dx.doi.org/10.1158/0008-5472.can-07-2559.